論文 / 著書情報
Article / Book Information

Title	Performance of sheet pile to mitigate liquefaction-induced lateral spreading of loose soil layer under the embankment
Authors	Partha Saha, Kazuki Horikoshi, Akihiro Takahashi
Citation	Soil Dynamics and Earthquake Engineering, Vol. 139, 106410
Pub. date	2020, 12
DOI	http://dx.doi.org/10.1016/j.soildyn.2020.106410
Creative Commons	See next page.
Note	This file is author (final) version.

License

Title:

Performance of sheet pile to mitigate liquefaction-induced lateral spreading of loose soil layer under the embankment

Authors:

Partha Saha

Graduate student, Department of Civil and Environmental Engineering, Tokyo Institute of Technology

Kazuki Horikoshi

Assistant Professor, Department of Civil and Environmental Engineering, Tokyo Institute of Technology

Akihiro Takahashi*

Professor, Department of Civil and Environmental Engineering, Tokyo Institute of Technology

* Corresponding author

Soil Dynamics and Earthquake Engineering, 139, 106410, 2020

Official URL:

https://doi.org/10.1016/j.soildyn.2020.106410

Abstract

Liquefaction-induced lateral spreading of the foundation soil severely damages the embankment resting on it. Installation of sheet pile near the toe of the embankment is a widely used technique to mitigate lateral spreading of the foundation soil and the associated damage to the embankment. However, several factors, such as the thickness of the liquefiable foundation, width of sheet pile, and softening of the bearing stratum, that may affect the performance of the sheet pile as seismic retrofit against lateral spreading has not been well studied yet. Therefore, a series of dynamic centrifuge experiments are carried out to study the applicability of sheet pile in various thickness of liquefiable foundation under moderate to strong sequential ground motions. It is found that the sheet pile effectively mitigates the lateral spreading of a thin as well as thick liquefiable foundation. Besides, the sheet pile having the same width of the target area performs equally as a wider sheet pile in mitigating channel-ward ground movement. The experimental results also show that the liquefaction-induced softening of the dense bearing stratum immediately below the loose foundation significantly influences the performance of the sheet pile.

Keywords

Centrifuge experiment; Embankment; Lateral spreading; Liquefaction; Sheet pile

1. Introduction

Liquefaction-induced lateral spreading causes massive damage to the structures. A large number of earthen structures, for example, river dykes, levees, dam, and road embankments are observed to fail severely during past earthquakes[1][2][3]. Several experimental and numerical studies have also been conducted to investigate the seismic failure of the embankment and the influence of the liquefiable foundation soils and its non-homogeneity [4][5][6]. The post-earthquake survey and the experimental studies reported that the liquefaction of the foundation soils likely causes the seismic damage of the earthen embankment. Therefore, the mitigation of liquefaction-induced lateral spreading of the foundation soil, which could potentially reduce the seismic damage of the embankment, is the focus of this study.

Liquefaction is the phenomenon of saturated sand which causes a significant loss of shear strength of soil due to the generation of excess pore water pressure. Extensive researches have been conducted on the remedial measures against liquefaction-induced damages. The remedial measures are broadly divided into two types; a) prevention of the liquefaction using ground improvement and b) reduction of the ground deformation using reinforcement. The ground improvement techniques, i.e. ground densification, is reported as a potential remedial measure for liquefaction-induced damages in the previous earthquakes[7][8][9] which is also confirmed in experimental and numerical studies [10][11][12][13]. The stone column is another densification technique commonly used for liquefaction mitigation[14][15]. The stone column technique densifies the surrounding soil, and at the same time, it provides vertical drainage for the dissipation of excess pore water pressure. The use of ground densification technique may not be suitable for the existing structures without interrupting its facilities. The

chemical stabilization using colloidal silica may be one of the techniques that can be applied to the existing structures[16]. Centrifuge experiments, as well as the field tests, show that the colloidal silica can mitigate the liquefaction of the ground, thus reducing the associated damages [16][17][18]. Since the colloidal silica solution in this method is transported through the soil matrix by permeation, uniform dispersion near a river may not be easy because of the contribution of the seepage flow from the water body.

The sheet pile is one of the reinforcement techniques commonly used to prevent the lateral spreading of the liquefied soil. Application of sheet pile to prevent the lateral spreading of the foundation soil under existing houses or earthen dykes/embankments has been studied before [19][20][21][22][23][24][25]. The sheet pile in all these cases can significantly reduce the lateral spreading of the subsoil irrespective of the type of superstructures. The sheet pile is usually installed near the toe of both sides of the embankment to prevent the lateral spreading of the foundation soil. The heads of the sheet pile installed at the opposite sides of the embankment are recommended to tie together to enhance its mitigation effects [26]. Besides, the liquefaction of the loose foundation soil inside sheet piles confinement provides base isolation thus reduce the seismic demand of the embankments[11][13]. Motamed and Towhata [27] installed a fixed-end sheet pile in between the quay walls and the pile groups to prevent the failure of the pile group caused by lateral spreading. The installation of sheet pile efficiently reduced the bending moment of the pile groups as well as the lateral spreading of the ground. The observation of the previous studies shows that the sheet pile technology could be a potential remedial measure against liquefaction-induced lateral spreading under the existing structures.

This study focuses on an effective remedial measure to mitigate liquefaction-induced lateral spreading of the loose soil layer under an existing approaching embankment of a river spanning bridge. The ground improvement techniques may not be feasible here, as it is mentioned before. Therefore, the authors consider sheet piles as a potential remedial measure in this case. Besides, the fixed-end sheet pile is almost impossible to achieve in reality. Therefore, the performance of a sheet pile to prevent the lateral spreading of the loose ground is studied here where the sheet pile tip is embedded into the underlying dense ground. Moreover, this study focuses on the performance of sheet pile in various thicknesses of the liquefiable layer, which has not been well studied yet. It is worth mentioning that the effect of bridge abutment is omitted for these series of experimental setups.

This paper describes the dynamic centrifuge experiments conducted on different foundation and reinforcement conditions. Two experiments are benchmark experiments where the embankment is constructed over a thick and thin liquefiable layer without any reinforcement. The sheet pile reinforcement is used in another three experiments for both the thick and the thin liquefiable layers. The geometry of the embankment remains same in all the experiments. The dynamic response of the ground, characterised by the surface settlement of the embankment, and lateral movement of the embankment and liquefiable foundation, are compared between the reinforced and unreinforced cases under the action of sequential ground motions.

2. Test conditions and procedures

2.1. Test conditions

Five centrifuge experiments are carried out at 50 g using the Tokyo tech Mark III centrifuge facility [28] to examine the applicability of sheet pile as a seismic retrofit against the liquefaction-induced lateral spreading. A sheet pile is used in this study as an indirect reinforcement to mitigate the lateral spreading of the foundation soil. The typical experimental setup consists of a loose liquefiable sand layer (Dr=50%) over a dense sand layer (Dr=90%), supporting an approach embankment. Generally, the embankments are compacted up to some desired level during the construction in reality. However, a loose embankment is used in this experiment to avoid densifying the loose foundation layer. Test conditions are summarised in Table 1. Two centrifuge experiments are carried out without any reinforcement to examine the effect of the liquefiable layer thickness on the deformation pattern of the ground. The thickness of the liquefiable layers is 8 m in C-1, and 4 m in C-2 in the prototype. The detailed experimental setup for C-1 and C-2 is shown in Fig. 1 and the applied scaling law is explained later. Since a river spanning bridge is assumed to be located around section X1, all the sensors are placed at section X1. A sheet pile is used as a mitigation measure in the other three experiments where the thickness of the loose foundation layer is 8 m in C-3 and 4 m in C-4 and C-4S in the prototype. The sheet pile tip is installed deep into the dense ground while the other end is extended into the slope of the embankment passing through the loose liquefiable sand layer as shown in Figs. 2 and 3. To observe the effect of the width of the sheet pile, C-4S is conducted with limited width (5 m in prototype) sheet pile. Whereas, a full-width sheet pile is used in C-3 and C-4. It is to be mentioned here that the half-width of the sheet pile is modelled in C-4S to observe the ground deformation at the middle of the protected area visually from the side window.

2.2. Preparation of the model ground

A rigid container, having the inner dimensions of 600 mm × 250 mm × 400 mm in length, width, and height, respectively, is used to prepare the model ground. The model ground is prepared with Toyoura sand. The physical properties of Toyoura sand are listed in Table 2. The air pluviation method is used to prepare the model ground with the desired relative density. The sheet piles are usually driven into the ground in reality. Whereas, the sheet piles during the model preparation are placed inside the container first. The sands are deposited afterwards for ease of construction and avoiding excessive densification of the surrounding soils during the preparation at 1 g. 2.5 mm thick steel plate is used here as a sheet pile. Both ends of the sheet pile are kept free to make the dynamic response more comparable to the real sheet pile. The specifications of the sheet pile in model scale and prototype are tabulated in Table 3. Three separate steel plates are used in these experiments to accommodate different widths. The width of the target area that needs to be protected is 50 mm (in model scale) from the container wall. A 50 mm width steel plate is installed at that location in C-4S where the soil beside the steel plate is allowed to move freely. Whereas, in the cases of full-width sheet pile (C-3 and C-4), two additional plates are added beside the 50 mm width steel plate to mitigate the lateral spreading in the full-width. Two different configurations of sheet pile are used in C-4 and C-4S to investigate whether the uneven lateral spreading of the surrounding ground affects the response of the target area. The steel plates in C-3 and C-4 are jointed together with rubber strips, and the joints are sealed with water repellent material to prevent the flow of fluid between the adjacent sections separated by sheet pile. Different stages of model ground preparation are depicted in Fig. 4.

Once the construction of the model ground is finished, the model ground is placed inside an airtight chamber with 760 mm Hg vacuum pressure to saturate with the de-aerated Metolose (60 SH-50) solution (2.2% by weight) to make the viscosity of the pore fluid 50 times of water. Metolose (60SH-50), the commercial name of Hydroxypropyl Methylcellulose from Shin-Etsu Chemical Company, is mixed with water at a specified proportion to increase the viscosity [29] of the solution by keeping the density and surface tension nearly identical to water. Metolose solution is dripped slowly from the top of the model ground and allowed to permeate through the soil media towards the bottom of the container. Thus, the model ground is gradually saturated with the viscous Metolose solution. The model ground is taken out of the vacuum chamber after the saturation of the foundation layers is completed. An embankment is then constructed over the saturated ground. A river approaching embankment is replicated in this experiment. Therefore, the embankment having one side slope (1:2) towards the river channel is prepared as shown in Figs. 1-3.

Accelerometers, pore pressure gauges, potentiometer, and Laser Displacement Transducers (LDT) are installed to monitor the response of the ground. The accelerometers and the pore pressure gauges are installed during the preparation of the model ground. Several white colour markers made of a small nail are placed at different levels inside the model ground, as shown in Fig. 4 to track the ground deformation at different layers after the application of sequential ground motions. The sensors are arranged in three lines inside the model, as shown in Figs. 1-3. The sensors in Line-1 and Line-3 are located under the embankment and inside the river channel, respectively. Whereas, the sensors in Line-2 are located under the slope of the embankment. The potentiometers are placed to monitor the settlement of the embankment surface. The LDTs are installed to track the horizontal movement at the slope.

136

137 *2.3. Applied ground motions*

138 Two successive ground motions applied to the model ground are shown in Fig. 5. The model
139 ground first experiences the Tohoku ground motion. The second ground motion consists of
140 sinusoidal waves having a frequency of 1.42 Hz with a maximum amplitude a_{max} = (0.48 - 0.51)
141 g. The sinusoidal waves are applied when the excess pore water pressure developed during
142 the first ground excitation is dissipated completely. One of the purposes of applying the
143 sinusoidal waves is to visualize the ground deformation more clearly. For this purpose, a high
144 frequency and high amplitude sinusoidal waves are applied to the model ground. The first
145 motion is similar to the actual one in the Tohoku Earthquake recorded at the ground surface
146 near the New Bansuikyo Bridge, Tochigi (2-I-I-3, NS component), but the magnitude is
147 comparatively smaller. However, the first ground excitation applied to the model ground will
148 be regarded as the Tohoku Earthquake throughout this paper.

149 In order to check the repeatability of the applied ground motions, the Arias intensity [30] of
150 the applied ground motions in all the cases is compared for both Tohoku Earthquake and
151 sinusoidal waves. Arias intensity represents the amount of energy applied to the model
152 ground. The Arias intensity of Tohoku Earthquake and sinusoidal waves for all five cases are
153 compared in Fig. 6. The figure shows that the Arias intensity of the applied ground motion in
154 all the cases is almost similar, which indicates the repeatability of the input ground excitation.

155

156 *2.4. Scaling laws used in the experiments*

157 The experiments are conducted under the 50 g environment. In order to accommodate a large
158 prototype within the limited dimensions of the centrifuge, a generalised scaling law [31] is

applied here. A 1:2 scaled shake table experiment is considered to perform under the 50 g environment. Therefore, a scaling law for the 1 g shake table experiment along with a scaling law for the 50 g centrifuge is applied together while designing the experimental model. The scaling factors used in the experiments for different important parameters are tabulated in Table 4. As for the viscosity of the pore fluid, if we follow the generalised scaling law, it should be 70.71 times of water. However, due to difficulties in saturating the model ground with larger viscosity fluid, the viscosity of the pore fluid is set 50. Thus, the permeability of the soils is rather large, and the relatively faster dissipation of the excess pore water pressure is expected.

3. Test results and discussion

The dynamic response of saturated ground predominantly depends on the generation of excess pore water pressure and the propagation of the seismic wave. In the following, the ground response to the seismic excitations is described and discussed. All the results in this paper are presented in the prototype scale unless mentioned otherwise.

3.1. Excess pore water pressure evolution

The soil is considered to be liquefied when the excess pore water pressure (Δu) reaches the initial vertical effective stress (σ_o'). In other words, the liquefaction takes place when the excess pore pressure ratio $r_u = \Delta u / \sigma_o'$ approaches to unity. Pore pressure gauges are placed at different depth under the embankment (P1-7, P1-5 and P1-3), under the soil slope (P2-7, P2-5 and P2-3), and inside the river channel (P3-7, P3-5, and P3-3) to observe the evolution of excess pore water pressure at different locations. Seismic response of the soil inside the river

channel significantly influences the ground movement under the embankment. Therefore, the excess pore water pressure time histories inside the river channel (P3-3, P3-5 and P3-7) for the benchmark cases C-1 and C-2 are shown in Fig. 7 and Fig. 8, respectively.

The pore pressure gauges P3-3 is located in the middle of the liquefiable layer. The r_u value is observed to reach 1.0 at 71.6 s and 61.6 s in C-1 and C-2, respectively during the Tohoku Earthquake, which is 28.0 s and 27.1 s, respectively during sinusoidal waves. It refers that the locations near the surface are liquefied earlier than the deeper locations in the free field. The liquefaction in the dense layer is also observed in the experiments. The pore pressure gauges P3-5 and P3-7 are placed inside the dense layer. P3-5 is located 11.5 m and 8.5 m below the river channel surface in C-1 and C-2, respectively. The r_u value reaches 1.0 at 85.0 s in C-1 while the dissipation of the excess pore water pressure starts immediately after that. Whereas, the liquefaction starts at 80.0 s in C-2 that continues until 128.0 s. The sinusoidal waves cause the liquefied state of the dense layer at P3-5 to continue even after the shaking, which is true for all the cases. The deeper dense layer (P3-7) is not liquefied during the Tohoku Earthquake. The maximum r_u values measured at P3-7 are 0.6 and 0.7 in C-1 and C-2, respectively. However, the sinusoidal waves cause liquefaction in the deeper dense layer as well. The seismic response of the layered ground in the river channel depicts that the dense sand (Dr = 90%) can also liquefy under the action of strong ground motion. Similar behaviour is also reported by Zeng and Liu [32]. Besides, the dense soil just below the loose liquefiable layer is found more susceptible to liquefaction than the deeper dense layer.

Figure 9 presents the excess pore water pressure time histories in the middle of the liquefiable layer under the embankment (P1-3) for C-1 and C-2. The figure shows that the maximum r_u value is about 0.5 in C-2 whereas the maximum r_u in C-1 reaches 0.9 with larger fluctuation

205 during the Tohoku Earthquake. Similarly, during the sinusoidal waves, the r_u value in C-2 is
206 lower than 1.0, whereas, the middle of the liquefiable layer in C-1 almost get liquefied.
207 Compared to the river channel, the state is relatively far from the liquefaction, probably
208 because of the confinement provided by the embankment. The shear strain time histories,
209 calculated at the middle of the liquefiable layer under the embankment and inside the river
210 channel during the Tohoku Earthquake, are shown in Fig. 10 for C-1. The shear strain of a soil
211 layer is calculated from the acceleration time histories recorded at the bottom and the top of
212 the layer at that corresponding location as described in Elgamal et al. [33]. The shear strain in
213 the liquefiable layer under the embankment is significantly smaller in magnitude than the
214 shear strain at the middle of the liquefiable layer inside the river channel. A smaller shear
215 strain in the liquefiable layer under the embankment, probably because of the confinement
216 provided by the embankment, prevents the soil to reach the liquefied state.

217 Figure 11 shows the excess pore water pressure time histories at the middle of the liquefiable
218 layer under the embankment slope for C-2, C-4 and C-4S. The excess pore water pressure for
219 both the unreinforced (C-2) and the reinforced cases (C-4 and 4S) are shown here. The figure
220 shows the loose soil under the embankment slope in C-2 almost reaches the liquefied state
221 during the Tohoku Earthquake, whereas, the soil gets liquefied during the sinusoidal waves.
222 The excess pore water pressure in the unreinforced (C-2) and reinforced (C-4 and C-4S) cases
223 is almost similar which is true for the response observed inside the river channel and under
224 the embankment as well. The pore pressure gauges under the embankment slope are installed
225 5 m away from the sheet piles. It implies that the response at the zone far from the sheet piles
226 is probably insignificantly influenced by the sheet piles. Unfortunately, as the excess pore
227 water pressure at P2-3 in C-3 cannot be recorded because of the malfunctioning of the pore

pressure gauge during the experiment, the comparison between the unreinforced and the reinforced cases with thick liquefiable layer cannot be made here.

3.2. Ground deformation without reinforcement

The centrifuge experiments can successfully produce the liquefaction-induced lateral spreading of the liquefiable soil both in the cases of the thick and thin liquefiable layer. A significant channel-ward movement of the liquefiable foundation soil, as well as the approach embankment, is observed. An attempt is made to show the ground deformation pattern using PIV (Particle Image Velocimetry) analysis [34]. The embankment slope and the underlying loose foundation is focused in this analysis since the major lateral spreading is observed in this region. The region of PIV analysis in the model ground for C -1 and C-2 is shown in Fig. 12. A smaller area is covered in C-2 because of the insufficient light outside of this region. Figures 13 and 14 show the ground deformation for C-1 and C-2, respectively. All the figures shown here are plotted in the model scale. The movement of the soil at several locations cannot be properly detected in PIV analysis due to the optical obstruction caused by scotch tape attached to the glass window. The displacement vectors at those locations have been removed and left it blank in the figures.

The displacement vectors in PIV results show that dry loose soil in the embankment slope moves horizontally as well as goes under a significant settlement. On the other hand, the channel-ward movement is dominant in the loose foundation soil layer. A heaving near the toe of the embankment is also observed especially in the case of thick loose foundation soil layer (C-1) under the strong ground motion of sinusoidal waves. The graphs show that the sinusoidal waves, in comparison with the Tohoku Earthquake, cause a larger ground

deformation of the loose embankment as well as a larger lateral spreading of the liquefiable foundation.

3.3. Performance of sheet pile to mitigate lateral spreading of liquefiable soil

The sheet pile is used to mitigate the liquefaction-induced lateral spreading of the ground. It is expected that the sheet pile installed deep into the dense ground will perform as a cantilever retaining structure that can prevent or reduce the channel-ward movement of the liquefied soil and the associated deformation of the embankment. The horizontal and vertical displacements at two locations on the embankment slope (TR-1 and TR-2) are measured and compared, as shown in Fig. 15.

The term “V” and “H” inside the brackets in Fig. 15 represents the vertical and horizontal displacement of the targets, respectively. The results show that the sheet pile can reduce the lateral displacement nearly up to 50% in the case with the thick liquefiable layer (C-3) and 30% in the case of a thin liquefiable layer (C-4 and C-4S) in the middle of the slope (TR-2). Limited width of the ground is protected in C-4S. The soil beside the sheet pile is left unprotected. The unprotected ground aligned in the same position with the sheet pile in the transverse direction (in C-4S) is observed to have larger channel-ward movement than the sheet pile. However, the ultimate horizontal displacement at the head of the sheet pile in C-4 and C-4S is almost similar during the Tohoku Earthquake as well as in sinusoidal waves. It implies that the lateral spreading of the unprotected ground beside the sheet pile doesn’t affect its performance much. Therefore, the performance of the limited width sheet pile (C-4S) and the full-width sheet pile (C-4) is almost similar in terms of preventing the lateral displacement of the ground. The result shows that the sheet pile effectively reduces the lateral spreading

under sequential ground motions. One of the purposes of the application of sequential ground motion is to observe the applicability of sheet pile if the target structure experiences two strong ground motions. The primary focus is the total reduction of the lateral spreading by the sheet pile. Therefore, the difference in the ground condition between the reinforced and unreinforced model before the application of the sinusoidal waves is not considered during the comparison of the experimental results.

A comparison of the ground deformation (at TR-1) between the unreinforced and reinforced cases during the Tohoku Earthquake is shown in Fig. 16. The figure shows that the embankment slope starts to deform with the generation of the excess pore water pressure in the middle of the liquefiable layer under the embankment nearly at 60.0 s. The ground deformation stops immediately after the dissipation of the excess pore water pressure starts at 90.0 s. Since no significant post liquefaction settlement or post-earthquake ground movement is observed, it can be said that the ground deformation is driven by the combination of the cyclic and static shear stress. Installation of the sheet pile can considerably reduce the horizontal movement of the embankment slope for all the cases. However, the vertical settlement of the embankment slope (TR-1 (V)), especially in the cases of the thin liquefiable layer (C-4 and C-4S) cannot be significantly reduced. Vertical settlement of the target is almost similar in both reinforced and unreinforced cases. It implies that the settlement is predominantly caused by the compaction of the loose soil due to seismic excitation.

An attempt is made to quantify the lateral movement of the liquefied soil behind and in front of the sheet pile. A grid pattern made of vertical and horizontal coloured noodles, as shown in Fig. 17, are placed at the back of the glass window of the model container to monitor the

297 lateral spreading of the soil. The lateral displacement of the vertical noodles is manually
298 measured after the application of the sequential earthquakes. The displacements of four
299 different lines in Fig. 17 are measured and compared, as shown in Figs. 18 and 19 for the cases
300 of thick and thin liquefiable layer, respectively. The figures show that the maximum lateral
301 spreading of liquefied soil takes place in the thick liquefiable foundation (C-1), which is
302 significantly reduced by the installation of sheet pile (see Fig. 18). Similarly, the lateral
303 spreading of soil reinforced with sheet pile for the thin liquefiable layer cases (C-4 and C-4S)
304 is observed to be smaller in comparison with the unreinforced case (C-2), as shown in Fig. 19.
305 However, the reduction of the lateral displacement of soil, achieved due to the installation of
306 the sheet pile, decreases with the distance behind the sheet pile (see Figs. 18 and 19). In
307 general, installation of the sheet pile makes the horizontal displacement profile of the ground
308 rather straight. Because of this, the displacement in the liquefiable layer is suppressed, while
309 that in the dense layer just below the liquefiable layer becomes somewhat large.

310

311 *3.4. Bending moment of sheet pile*

312 The sheet pile is expected to experience a large bending moment caused by the forces from
313 destabilized soil due to liquefaction. The sheet pile having a 50 mm width (in model scale) is
314 instrumented with strain gauges at different depths to measure the bending moment.
315 Wheatstone half-bridge configuration is used to wire two strain gauges attached to the
316 opposite side of the sheet pile to get the bending strain only. The installation of strain gauges
317 along the surface of the sheet pile is shown in Fig. 20 (a). The sign convention of bending
318 moment used in this paper is shown in Fig. 20 (b).

The sheet pile experiences maximum bending moment around 86.0 s during the Tohoku Earthquake and 48.0 s during sinusoidal waves in all the three cases. A comparison of the bending moment profiles of the sheet pile in C-3, C-4, and C-4S, when the sheet pile experiences maximum bending moment, both under Tohoku Earthquake and sinusoidal waves is shown in Fig. 21. The forwards diagonal cross-hatched region in the figure represents the liquefiable layer for C-4 and C-4S, and the combination of forwards and backwards diagonal cross-hatched regions in the figure represents the liquefiable layer for C-3. The figure shows that the maximum bending moment takes place 4 m deep into the dense layer rather than the interface of the dense and the loose layer in C-4 and C-4S. The magnitude of the maximum bending moment in the thin liquefiable layer is almost similar in both cases with the full-width sheet pile (C-4) and limited width sheet pile (C-4S). Whereas, the maximum bending moment of sheet pile in the case of the thick liquefiable layer (C-3) is quite larger than the other cases because of the contribution of the thick liquefiable layer. However, the shapes of the bending moment distribution profile in all three cases are almost similar.

3.5. Earth pressure acting on the sheet pile

The sheet pile is expected to experience a significant earth pressure exerted by the build-up of excess pore water pressure and the spreading of the liquefied soil with the crust layer. The resultant earth pressure that represents the difference of the channel-ward pressure and the resisting pressure acting on the sheet pile is back-calculated from the bending moment distribution using the following equations.

$$p(z,t) = \frac{\partial^2 M(z,t)}{\partial z^2} \quad (1)$$

To estimate the resultant earth pressure, double differentiation of fitted polynomial curve through the discrete bending moment data points is one of the popular methods. However, double differentiation of a fitted polynomial curve may produce potential errors, especially near the ends of the structural elements that may mislead the value of the earth pressure. Therefore, the weighted residual method proposed by Brandenberg et al. [35] is used in this paper. The weighted residual method yields approximate solutions of a differential equation only valid at the boundaries which are assumed to produce less noise in comparison with the exact solution of continuous equations. Both ends of the sheet pile are kept free in the experiment, which yields zero shear force at that location. Therefore, a boundary condition is imposed on the solution that refers to the first derivative of the bending moment $\left(\frac{\partial M}{\partial z}\right)$ at the ends of the sheet pile will remain zero.

Lateral spreading is sometimes considered as a post-liquefaction phenomenon that may take place even after the earthquake stops. Therefore, the trend component of the bending moment is sometimes used to calculate the earth pressure caused by lateral spreading [36]. However, in this study, no post-earthquake ground movement is observed. Moreover, the contribution of the cyclic component to the maximum bending moment of the sheet pile especially in the event of the sinusoidal waves is found to vary from 20% (C-3) to 40% (C-4 and C-4S) of the trend component depending on the thickness of the liquefiable layer as shown in Fig. 22. The cyclic component is significantly large, which can change the earth pressure distribution as well. Therefore, the real-time bending moment data, combining both the cyclic and trend components, is used for further analysis.

The resultant earth pressure back-calculated from the measured bending moment data represents the difference of the channel-ward pressure and the resisting pressure acting on

364 the sheet pile. Resultant earth pressure profiles of the sheet pile during the maximum bending
365 event in C-3, C-4, and C-4S that takes place nearly at 86.0 s during the Tohoku Earthquake are
366 shown in Fig. 23. The negative value represents the resultant earth pressure acting towards
367 the backfill, and the positive value indicates the resultant earth pressure towards the river
368 channel. The resultant channel-ward earth pressure, acting on the upper part of the sheet pile,
369 is affected by the embankment and the liquefiable layer. The maximum resultant channel-
370 ward earth pressure imposed by the liquefiable layer is observed to increase proportionally
371 with its thickness.

372 Liquefaction inside the river channel causes a considerable softening of the soil thus reduces
373 the resistance provided by the channel-side soils. A plot of the resultant earth pressure time
374 histories at SP-3 and SP-4 along with the excess pore water pressure time histories of the
375 surrounding soil inside the river channel are shown in Figs. 24 and 25 for C-3 and C-4,
376 respectively. SP-3 (at a depth of 4 m from the liquefiable layer top) is located at the middle of
377 the liquefiable layer in C-3, and at the interface of the loose and the dense layer in C-4.
378 Whereas, SP-4 (at a depth of 8 m from the liquefiable layer top) is located at the interface of
379 the loose and the dense layer in C-3 and inside the dense ground in C-4. According to the pore
380 pressure gauge readings, in C-3 the liquefaction takes place from the surface to the depth
381 between P3-3 and P3-5 (around 8 m deep from the surface), while that was down to the depth
382 between P3-5 and P3-7 (around 8.5 m deep from the surface) in C-4. The figures show that
383 the resultant earth pressure towards the backfill, which is influenced by the liquefaction
384 extent of the channel-side soils at SP-3, gradually increases (the value in the figure decreases)
385 until 75.0 s in C-3 and 80.0 s in C-4 before the channel-side soils at that vicinity get liquefied.
386 However, once the soil gets liquefied, the resisting earth pressure is observed to decrease (the
387 value in the figure increases) because of the softening of the soil inside the river channel. On

388 the other hand, the resisting earth pressure at SP-4 is observed to increase (the value in the
389 figure decreases) gradually and reach a residual value since the supporting dense soils don't
390 liquefy.

391 The shear force distributions of the sheet pile at the cyclic peaks of 1st cycle and the maximum
392 bending event during the sinusoidal waves in all three cases (C-3, C-4 and C-4S) are shown in
393 Fig. 26. The peak in the first cycle takes place around 28.0 s when the loose layer in all three
394 cases get liquefied, whereas, the upper dense layer is yet to be liquefied. The shear force
395 distribution for the first cycle shows that it changes its sign at a depth of 4 m (from the top of
396 the liquefiable layer) in C-4 and 4S, and 7 m (from the top of the liquefiable layer) in C-3 that
397 represents the location of maximum bending moment at that event. However, the shear force
398 distribution when the sheet pile experiences the maximum bending changes its sign at a depth
399 of 9 m (from the top of the liquefiable layer) in C-3 and C-4 and 8 m (from the top of the
400 liquefiable layer) in C-4S. The liquefaction of the upper dense layer is responsible for these
401 considerable downward shifts of the location of the maximum bending moment from the first
402 cycle to the cycle of the maximum bending event, particularly in C-4 and C-4S. The liquefaction
403 of the upper dense layer significantly reduces its resistance to prevent the channel-ward
404 forces from the backfill. Thus, the location of the maximum bending moment moves to a
405 greater depth. It implies that the liquefaction of the shallow dense layer significantly
406 influences the response of the sheet pile.

407

408 **4. Conclusions**

409 A series of dynamic centrifuge tests were performed to investigate the performance of sheet
410 pile installed into the dense soil to mitigate the liquefaction-induced lateral spreading of the

loose foundation soils under the embankment. The performance of sheet pile was investigated for both thin (4 m) and thick (8 m) liquefiable foundations under the 8 m height embankment. Moreover, the effect of the width of sheet pile on its performance as a possible seismic retrofit for the embankment of a river spanning bridge was also investigated. Several conclusions can be drawn from the experimental results.

The model ground was observed to go under significant deformation because of the lateral spreading of the foundation soil as well as the compaction of the loose embankment in the unreinforced condition. The installation of sheet pile can effectively mitigate the liquefaction-induced lateral spreading during the moderate to strong ground motions and equally effective in various thicknesses of liquefiable foundation ranging from 4 m to 8 m. The sheet pile was observed to reduce the channel-ward ground movement up to 30 to 50% at its closer vicinity. The extension of the width of sheet pile beyond the target area doesn't have any additional advantage. The performance of limited width (5 m) sheet pile in terms of mitigating lateral spreading was found similar to that of the full-width sheet piles. The liquefaction of the dense layer just below the loose layer significantly affects the overall response of the sheet pile. It causes the location of the maximum bending moment of the sheet pile moves to a greater depth inside the dense layer. Therefore, the liquefaction susceptibility of the dense layer immediately below the loose layer should be considered in the determination of the sheet pile specifications.

Acknowledgements

This study was supported by the research grant from the Japan Iron and Steel Federation in FY2018-2019. The first author would like to acknowledge the financial support provided by

Monbukagakusho (Ministry of Education, Culture, Sports, Science and Technology) scholarship during his study in Japan. The authors are also indebted to Mr Sakae Seki for his continuous cooperation during the centrifuge experiments.

References

[1] Yegian MK, Ghahraman VG, Harutiunyan RN. Liquefaction and embankment failure case histories, 1988 armenia earthquake. J Geotech Eng 1994;120:581–96. https://doi.org/10.1061/(ASCE)0733-9410(1994)120:3(581).

[2] Matsuo O. Damage to river dikes. Soils Found 1996;36:235–40. https://doi.org/10.3208/sandf.36.Special_235.

[3] Sasaki Y, Towhata I, Miyamoto K, Shirato M, Narita A, Sasaki T, et al. Reconnaissance report on damage in and around river levees caused by the 2011 off the Pacific coast of Tohoku Earthquake. Soils Found 2012;52:1016–32. https://doi.org/10.1016/j.sandf.2012.11.018.

[4] Kokusho T. Water film in liquefied sand and its effect on lateral spread. J Geotech Geoenvironmental Eng 1999;125:817–26. https://doi.org/10.1061/(ASCE)1090-0241(1999)125:10(817).

[5] Aydingun O, Adalier K. Numerical analysis of seismically induced liquefaction in earth embankment foundations. Part I. Benchmark model. Can Geotech J 2003;40:753–65. https://doi.org/10.1139/t03-025.

[6] Maharjan M, Takahashi A. Liquefaction-induced deformation of earthen embankments on non-homogeneous soil deposits under sequential ground motions. Soil Dyn Earthq Eng 2014;66:113–24. https://doi.org/10.1016/j.soildyn.2014.06.024.

[7] Watanabe T. Damage to oil refinery plants and a building on compacted ground by the niigata earthquake and their restoration. Soils Found 1966;6:86–99. https://doi.org/10.3208/sandf1960.6.2_86.

[8] Ishihara K, Kawase Y, Nakajima M. Liquefaction Characteristics of Sand Deposits at an Oil Tank Site During The 1978 Miyagiken-Oki Earthquake. Soils Found 1980;20:97–111. https://doi.org/10.3208/sandf1972.20.2_97.

[9] Yasuda S, Harada K, Ishikawa K, Kanemaru Y. Characteristics of liquefaction in Tokyo Bay area by the 2011 Great East Japan Earthquake. Soils Found 2012;52:793–810. https://doi.org/10.1016/j.sandf.2012.11.004.

[10] Liu L, Dobry R. Seismic response of shallow foundation on liquefiable sand. J Geotech Eng 1997;123:557–66. https://doi.org/10.1061/(asce)1090-0241(1997)123:6(557).

[11] Adalier K, Elgamal AW, Martin GR. Foundation liquefaction countermeasures for earth embankments. J Geotech Geoenvironmental Eng 1998;124:500–17. https://doi.org/10.1061/(ASCE)1090-0241(1998)124:6(500).

[12] Okamura M, Matsuo O. Effects of remedial measures for mitigating embankment settlement due to foundation liquefaction. Int J Phys Model Geotech 2002;2:01–12. https://doi.org/10.1680/ijpmg.2002.020201.

[13] Adalier K, Aydingun O. Numerical analysis of seismically induced liquefaction in earth embankment foundations. Part II. Application of remedial measures. Can Geotech J 2003;40:766–79. https://doi.org/10.1139/t03-026.

[14] Adalier K, Elgamal A. Mitigation of liquefaction and associated ground deformations by stone columns. Eng Geol 2004;72:275–91. https://doi.org/10.1016/j.enggeo.2003.11.001.

[15] Asgari A, Oliaei M, Bagheri M. Numerical simulation of improvement of a liquefiable soil

layer using stone column and pile-pinning techniques. Soil Dyn Earthq Eng 2013;51:77–96. https://doi.org/10.1016/j.soildyn.2013.04.006.

[16] Conlee CT, Gallagher PM, Boulanger RW, Kamai R. Centrifuge modeling for liquefaction mitigation using colloidal silica stabilizer. J Geotech Geoenvironmental Eng 2012;138:1334–45. https://doi.org/10.1061/(ASCE)GT.1943-5606.0000703.

[17] Pamuk A, Gallagher PM, Zimmie TF. Remediation of piled foundations against lateral spreading by passive site stabilization technique. Soil Dyn Earthq Eng 2007;27:864–74. https://doi.org/10.1016/j.soildyn.2007.01.011.

[18] Gallagher PM, Conlee CT, Rollins KM. Full-scale field testing of colloidal silica grouting for mitigation of liquefaction risk. J Geotech Geoenvironmental Eng 2007;133:186–96. https://doi.org/10.1061/(ASCE)1090-0241(2007)133:2(186).

[19] Tanaka H, Kita H, Iida T, Saimura Y. Countermeasure for liquefaction using steel sheet pile with drain capability. 11th World Conf. Earthq. Eng. Pap. No. 1052, Acapulco, Mexico: Elsevier Science; 1996.

[20] Tanaka H, Murata H, Kita H, Okamoto M. Study on sheet pile wall method as a remediation against liquefaction. 12th world Conf. Earthq. Eng. Pap. No. 535, New Zealand: 2000.

[21] Kogai Y, Towhata I, Amimoto K, Putra HG. Use of embedded walls for mitigation of liquefaction-induced displacement in slopes and embankments. Soils Found 2000;40:75–93. https://doi.org/10.3208/sandf.40.4_75.

[22] Mizutani T, Towhata I. Model tests on mitigation of liquefaction-induced subsidence of dike by using embedded sheet-pile walls. Int. Conf. Recent Adv. Geotech. Earthq. Eng. Soil Dyn. 17, San Diego, California: University of Missouri--Rolla; 2001.

[23] Motohashi Y, Yasuhara K, Komine H, Murakami S. Mitigation of existing structure

505 settlement by sheet pile walls when liquefaction. Geotech. Spec. Publ., 2011, p. 1815–
506 20. https://doi.org/10.1061/41165(397)185.
507 [24] Rasouli R, Towhata I, Rattez H. Shaking Table Model Tests on Mitigation of Liquefaction-
508 Induced Distortion of Shallow Foundation. Geotech. Hazards from Large Earthquakes
509 Heavy Rainfalls, 2017, p. 463–77. https://doi.org/10.1007/978-4-431-56205-4_43.
510 [25] Yasuda S, Ishikawa K. Appropriate measures to prevent the liquefaction-induced
511 inclination of existing houses. Soil Dyn Earthq Eng 2018;115:652–62.
512 https://doi.org/10.1016/j.soildyn.2018.07.019.
513 [26] Adalier K, Pamuk A, Zimmie TF. Earthquake retrofit of highway/railway embankments
514 by sheet-pile walls. Geotech Geol Eng 2004;22:73–88.
515 https://doi.org/10.1023/B:GEGE.0000014000.27895.5d.
516 [27] Motamed R, Towhata I. Mitigation measures for pile groups behind quay walls
517 subjected to lateral flow of liquefied soil: Shake table model tests. Soil Dyn Earthq Eng
518 2010;30:1043–60. https://doi.org/10.1016/j.soildyn.2010.04.016.
519 [28] Takemura J, Kondoh M, Esaki T, Kouda M, Kusakabe O. Centrifuge model tests on
520 double propped wall excavation in soft clay. Soils Found 1999;39:75–87.
521 https://doi.org/10.3208/sandf.39.3_75.
522 [29] Adamidis O, Madabhushi GSP. Use of viscous pore fluids in dynamic centrifuge
523 modelling. Int J Phys Model Geotech 2015;15:141–9.
524 https://doi.org/10.1680/ijpmg.14.00022.
525 [30] Arias A. A measure of earthquake intensity. Seism. Des. Nucl. Power Plants, 1970, p.
526 438–83.
527 [31] Iai S, Tobita T, Nakahara T. Generalised scaling relations for dynamic centrifuge tests.
528 Geotechnique 2005;55:355–62. https://doi.org/10.1680/geot.2005.55.5.355.

529 [32] Zeng X, Liu G. Liquefaction of dense sand under earthquake loading. Geotech. Spec.
530 Publ., 2012, p. 1670–9. https://doi.org/10.1061/9780784412121.172.
531 [33] Elgamal AW, Zeghal M, Taboada V, Dobry R. Analysis of Site Liquefaction and Lateral
532 Spreading Using Centrifuge Testing Records. SOILS Found 1996;36:111–21.
533 https://doi.org/10.3208/sandf.36.2_111.
534 [34] White DJ, Take W a. GeoPIV: Particle Image Velocimetry (PIV) software for use in
535 geotechnical testing. Cambridge Univ Eng Dep Tech Rep 2002:15.
536 [35] Brandenberg SJ, Wilson DW, Rashid MM. Weighted Residual Numerical Differentiation
537 Algorithm Applied to Experimental Bending Moment Data. J Geotech
538 Geoenvironmental Eng 2010;136:854–63. https://doi.org/10.1061/(asce)gt.1943-
539 5606.0000277.
540 [36] Haeri SM, Kavand A, Rahmani I, Torabi H. Response of a group of piles to liquefaction-
541 induced lateral spreading by large scale shake table testing. Soil Dyn Earthq Eng
542 2012;38:25–45. https://doi.org/10.1016/j.soildyn.2012.02.002.
543

Tables

Table 1: Test conditions.

Test ID	Thickness of liquefiable layer (m)	Existence of sheet pile	Width of sheet pile (m)	Relative density (%)		
				Embankment	Loose foundation	Dense foundation
C-1	8.0	No	-	54	53	92
C-2	4.0	No	-	51	54	90
C-3	8.0	Yes	Full-width	54	50	90
C-4	4.0	Yes	Full-width	54	52	88
C-4S	4.0	Yes	5.0	53	52	92

Table 2: Physical properties of Toyoura sand.

Specific gravity	2.65
Maximum void ratio	0.973
Minimum void ratio	0.609
Mean diameter D_{50} (mm)	0.19
Uniformity coefficient C_u	1.32

Table 3: Specifications of sheet pile in model scale and prototype.

	Model	Prototype
Material type	Steel	Steel
Stiffness EI (N-m^2/m)	2.6×10^2	5.2×10^8
Target sheet pile	-	Hat-type & H-shape composite

Table 4: Scaling factors used in the experiments.

Quantity	Model
Length	$1/(50 \times 2) = 1/100$
Acceleration	$(50 \times 1) = 50$
Time (dynamic)	$1/(50 \times 2^{0.5}) = 1/70.71$
Stiffness EI (structure)	$1/(50^4 \times 2^5) = 5 \times 10^{-9}$
Stress	1/2

Figures

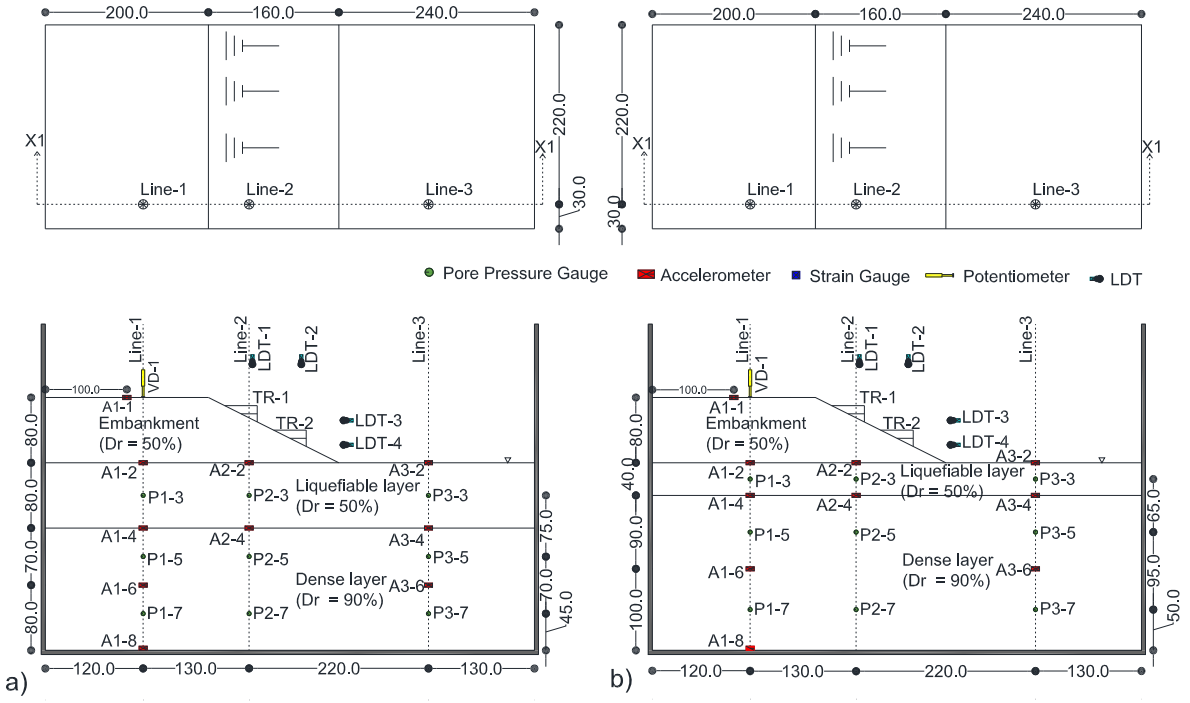

Fig. 1: Plan and cross-sectional view of a) C-1 and b) C-2 (all the dimensions are in mm in model scale).

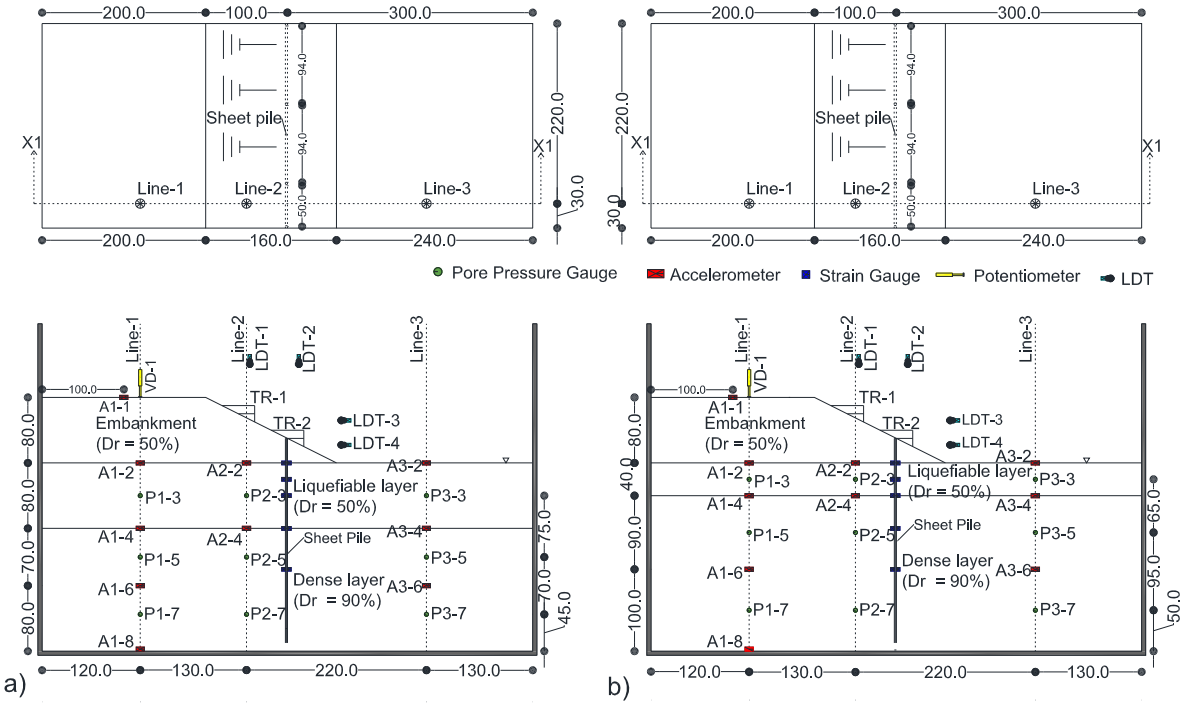

Fig. 2: Plan and cross-sectional view of a) C-3 and b) C-4 (all the dimensions are in mm in model scale).

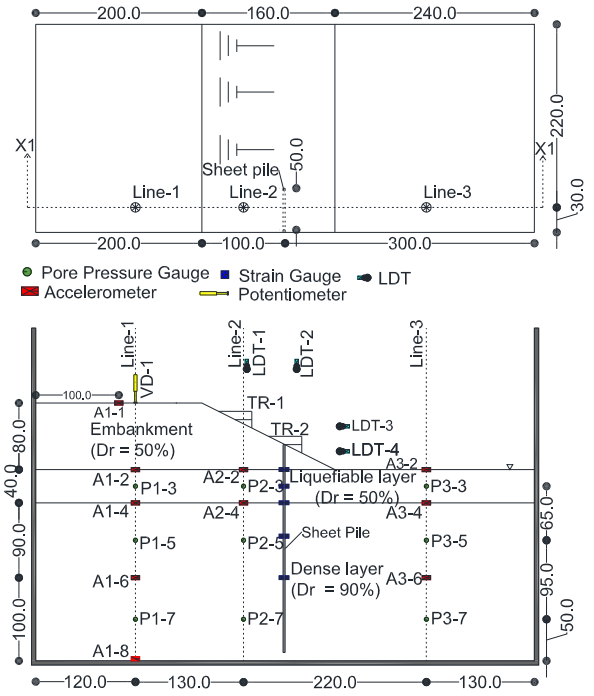

Fig. 3: Plan and cross-sectional view of C-4S (all the dimensions are in mm in model scale).

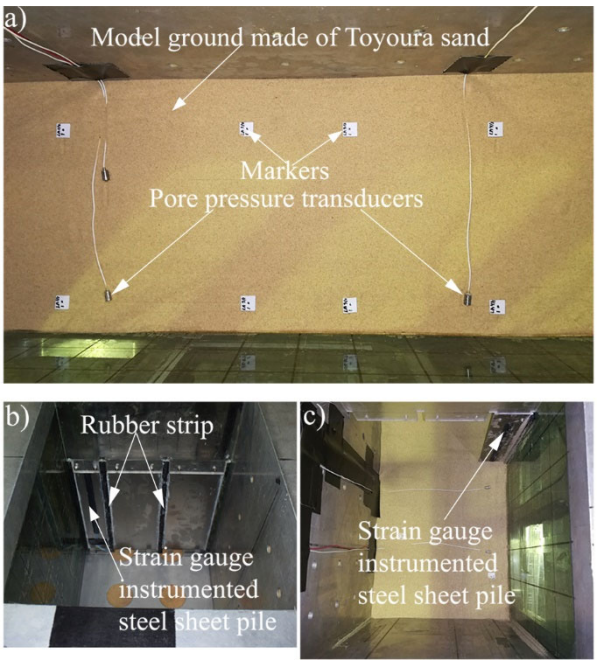

Fig. 4: Preparation of model ground; a) placement of sensors inside the ground, b) installation of sheet pile for full-width sheet pile, and c) installation of sheet pile for limited width sheet pile.

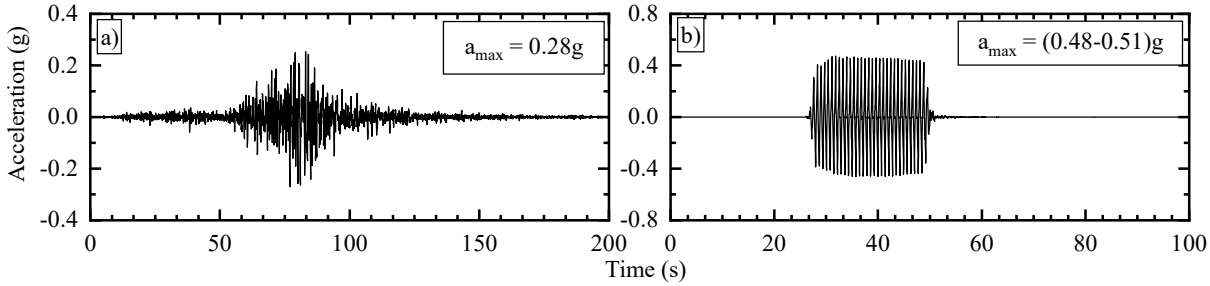

Fig. 5: Applied ground motions; a) Tohoku Earthquake and b) sinusoidal waves.

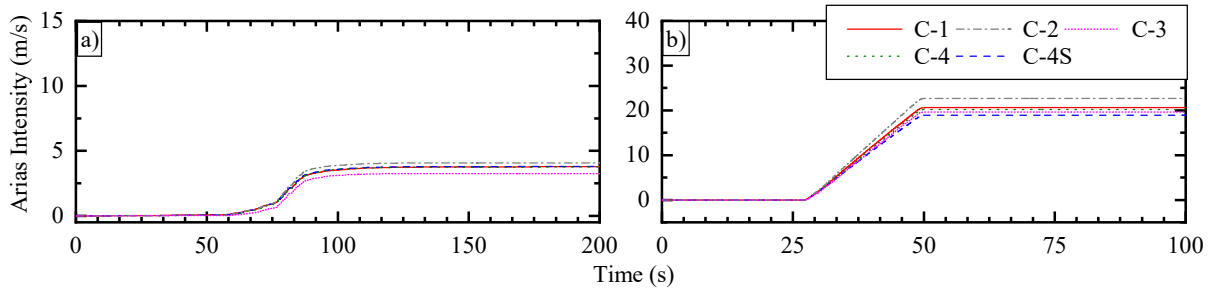

Fig. 6: Comparison of Arias intensity of input ground motions; a) Tohoku Earthquake and b) sinusoidal waves.

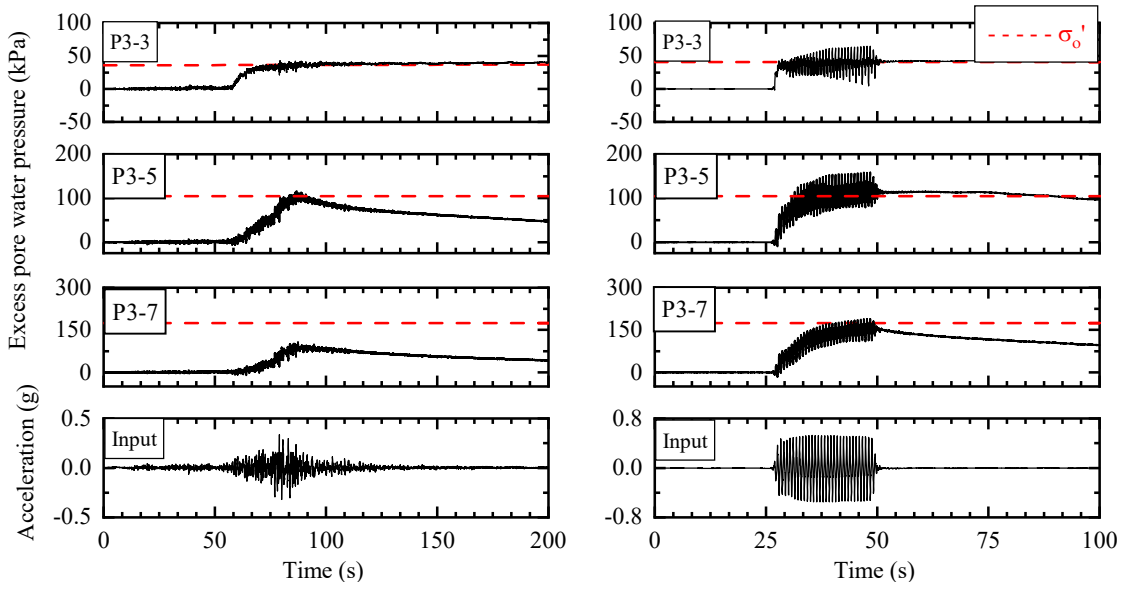

Fig. 7: Excess pore water pressure time histories inside the river channel in C-1 during Tohoku Earthquake (left column) and sinusoidal waves (right column).

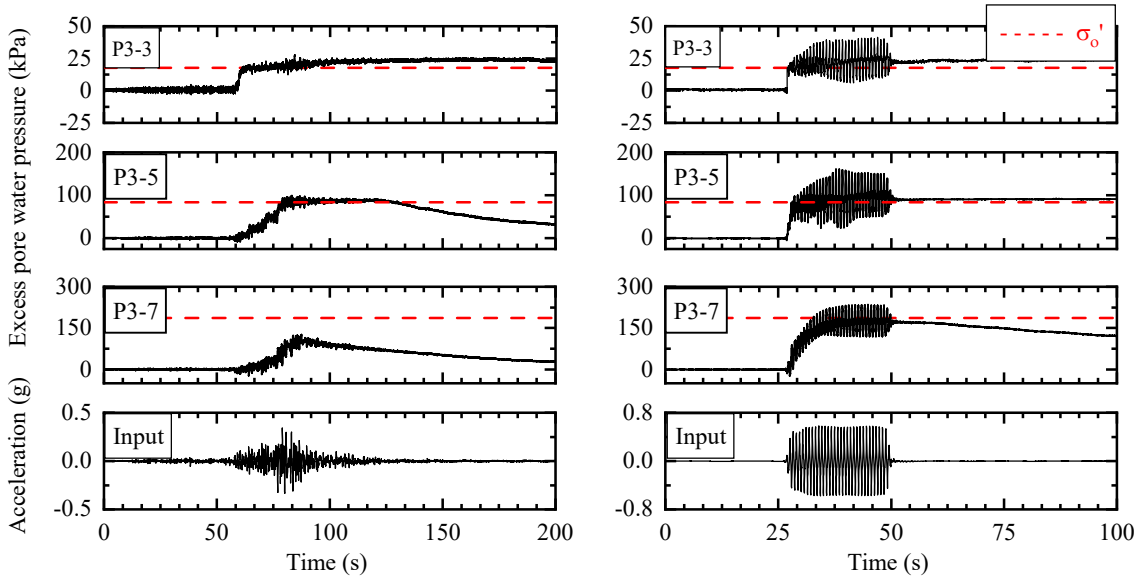

Fig. 8: Excess pore water pressure time histories inside the river channel in C-2 during Tohoku Earthquake (left column) and sinusoidal waves (right column).

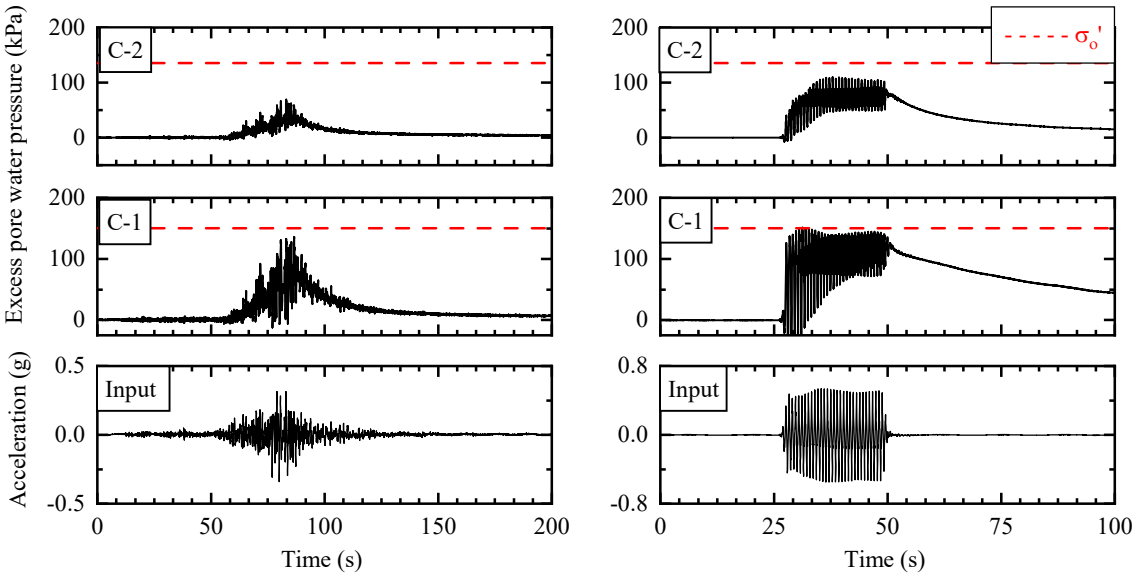

Fig. 9: Excess pore water pressure time histories at the middle of the liquefiable layer under the embankment (P1-3) in C-1 and C-2 during Tohoku Earthquake (left column) and sinusoidal waves (right column).

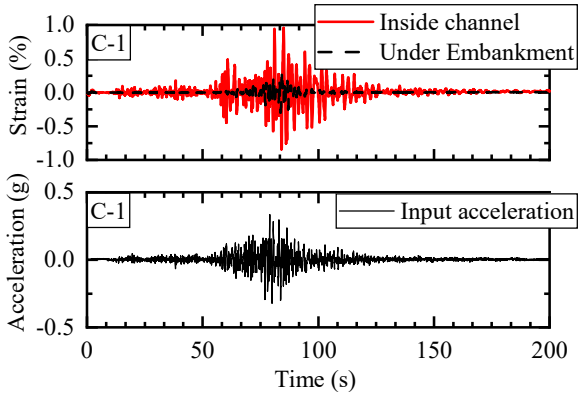

Fig. 10: Comparison of shear strain at the middle of the liquefiable layer inside the river channel and under the embankment in C-1.

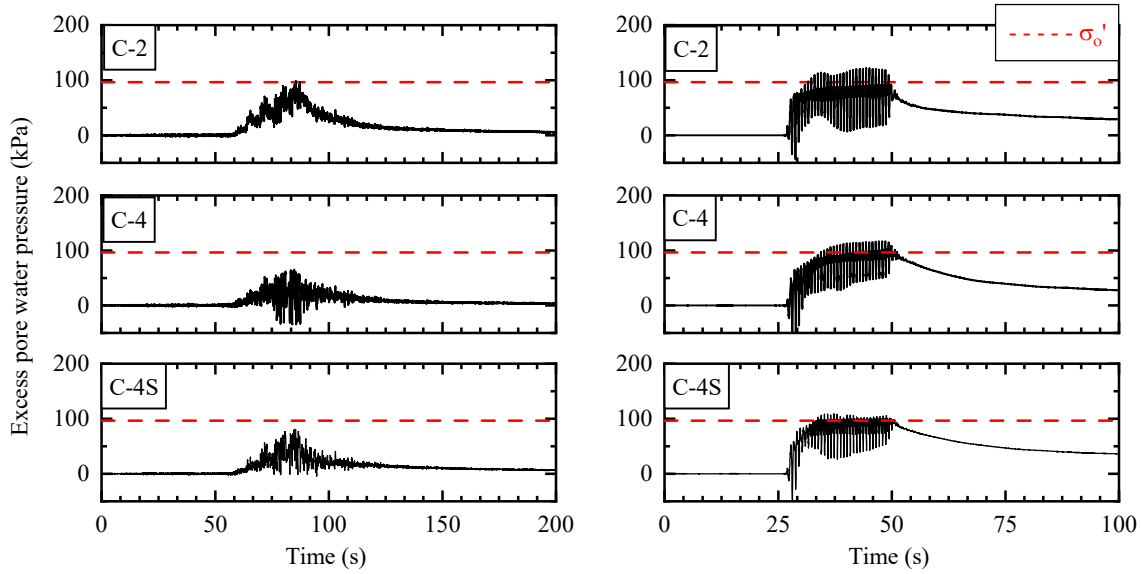

Fig. 11: Excess pore water pressure time histories at the middle of the liquefiable layer under the embankment slope (P2-3) in C-2, C-4 and C-4S during Tohoku Earthquake (left column) and sinusoidal waves (right column).

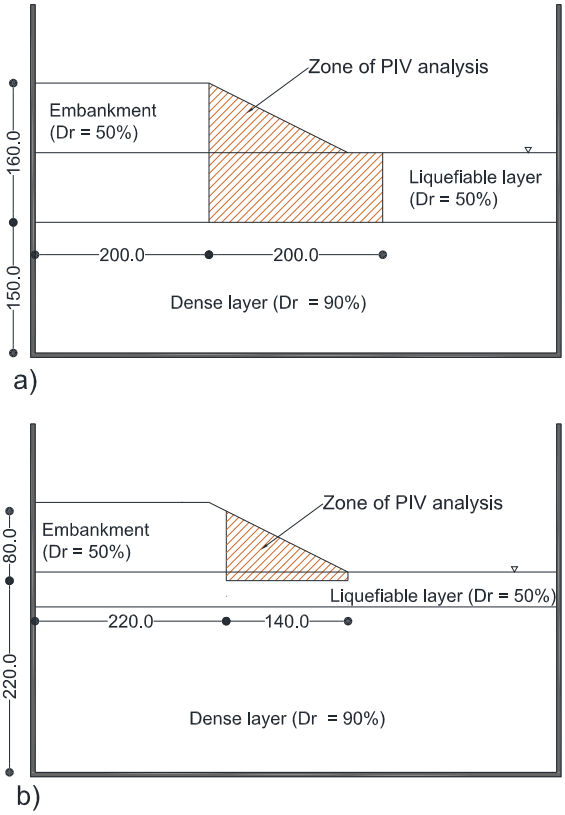

Fig. 12: Experimental model along with the zone of PIV analysis for; a) C-1 and b) C-2.

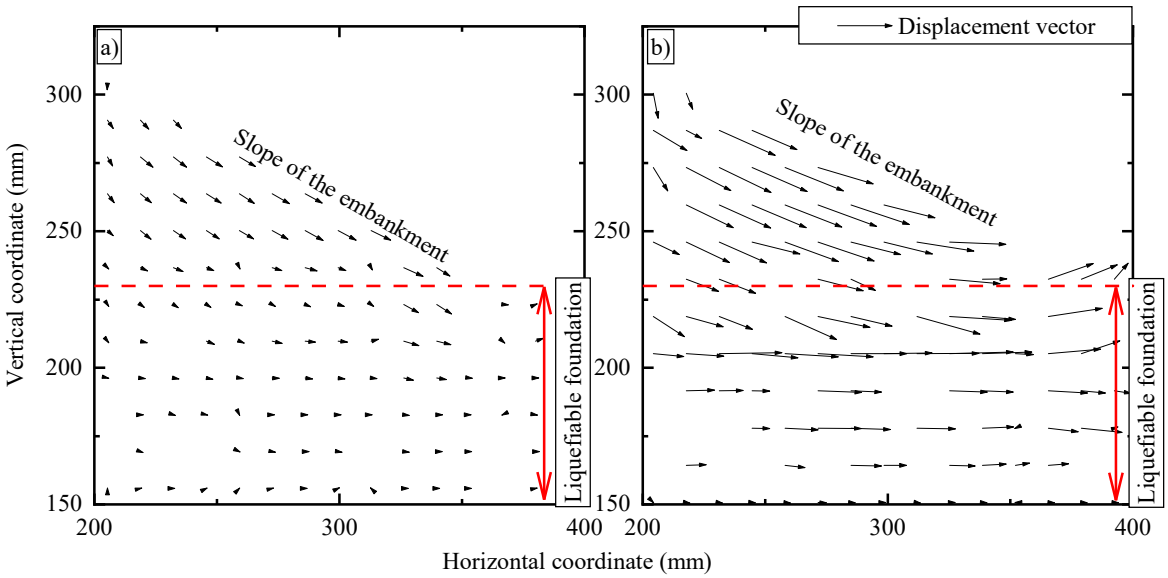

Fig. 13: Movement of the embankment slope and the loose foundation soil layer for C-1 in model scale; a) Tohoku Earthquake and b) sinusoidal waves.

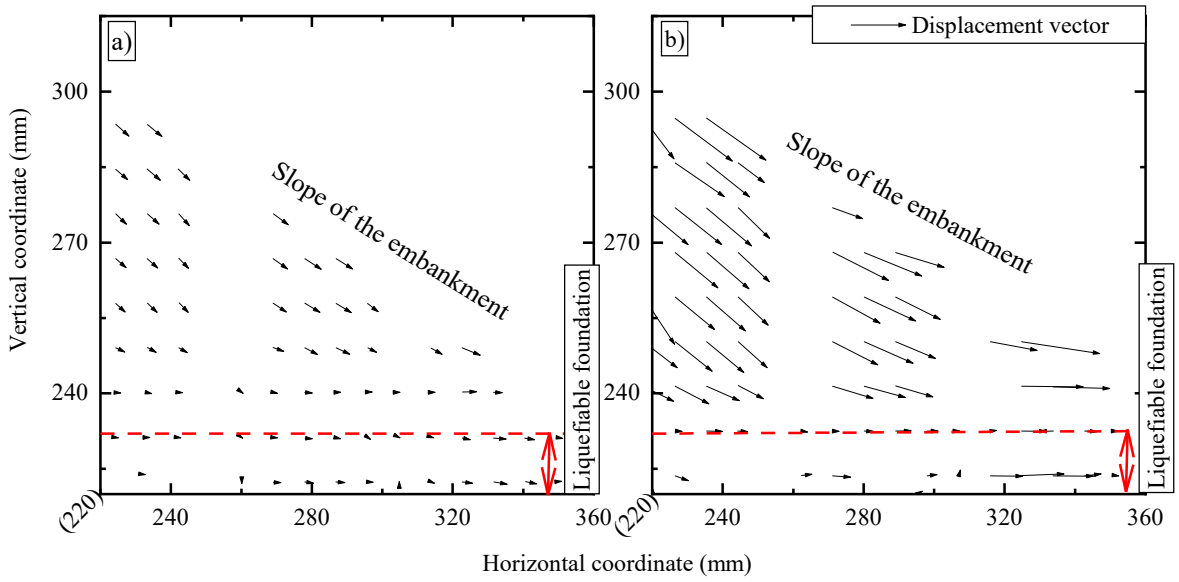

Fig. 14: Movement of the embankment slope and the loose foundation soil layer for C-2 in model scale; a) Tohoku Earthquake and b) sinusoidal waves.

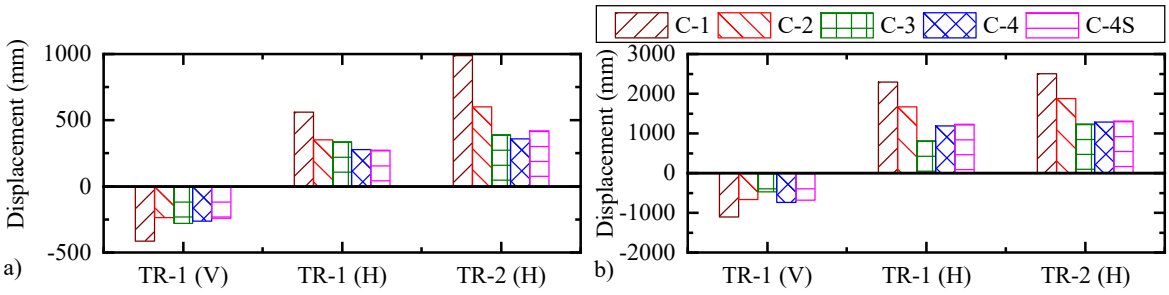

Fig. 15: Comparison of horizontal and vertical displacement of targets TR-1 and TR-2 among the reinforced and unreinforced cases; a) Tohoku Earthquake and b) sinusoidal waves.

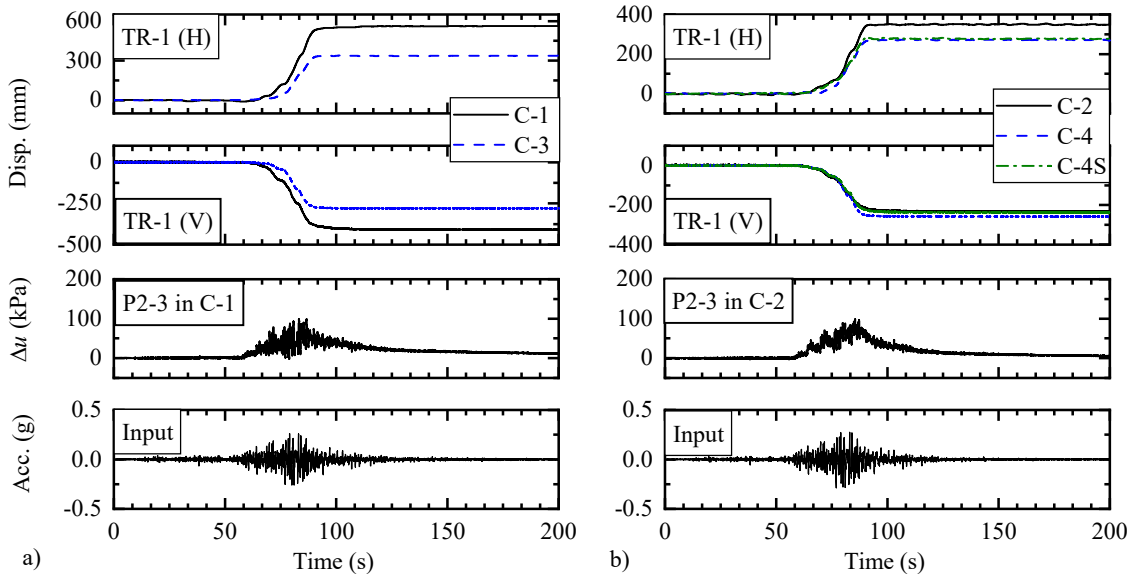

Fig. 16: Comparison of the ground deformation time histories at the slope of the embankment (TR-1) between the unreinforced and reinforced cases during Tohoku Earthquake; a) thick liquefiable layer (C-1 and C-3) and b) thin liquefiable layer (C-2, C-4 and C-4S).

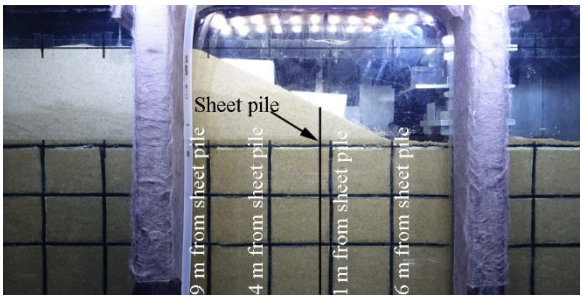

Fig. 17: Grid made of coloured noodles to observe the deformation of the ground.

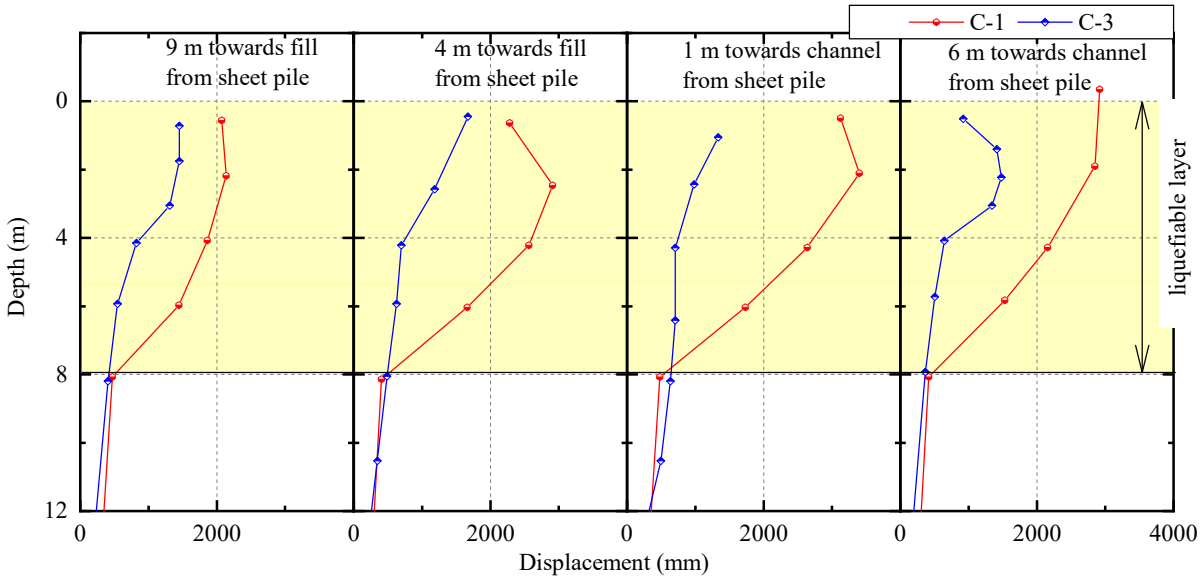

Fig. 18: Lateral displacement profiles of sand layers for the cases of thick liquefiable foundation (C-1 and C-3) (measured manually).

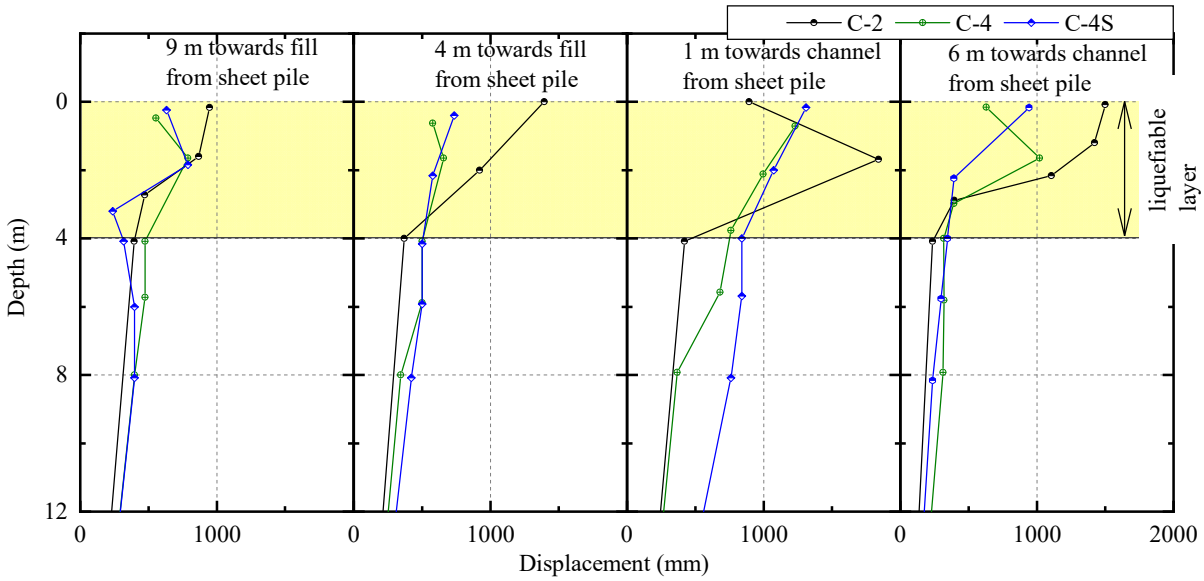

Fig. 19: Lateral displacement profiles of sand layers for the cases of thin liquefiable foundation (C-2, C-4 and C-4S) (measured manually).

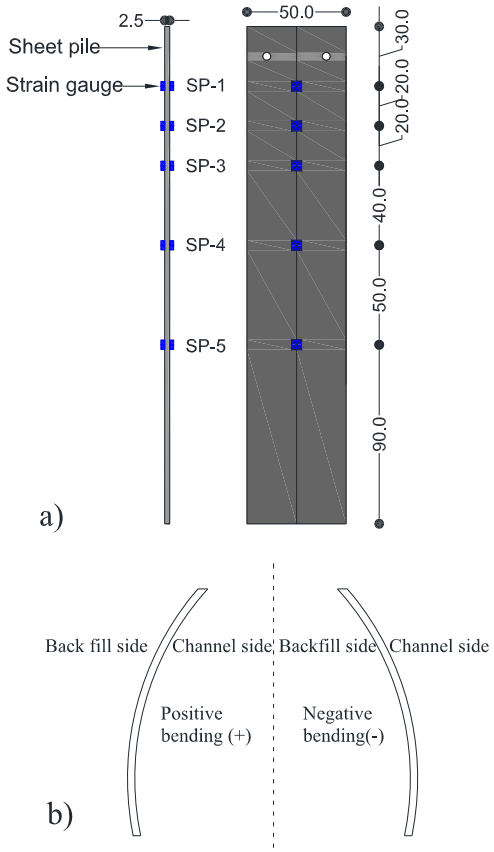

Fig. 20: a) Instrumentation of sheet pile with strain gauges (in model scale) and b) sign convention for bending moment.

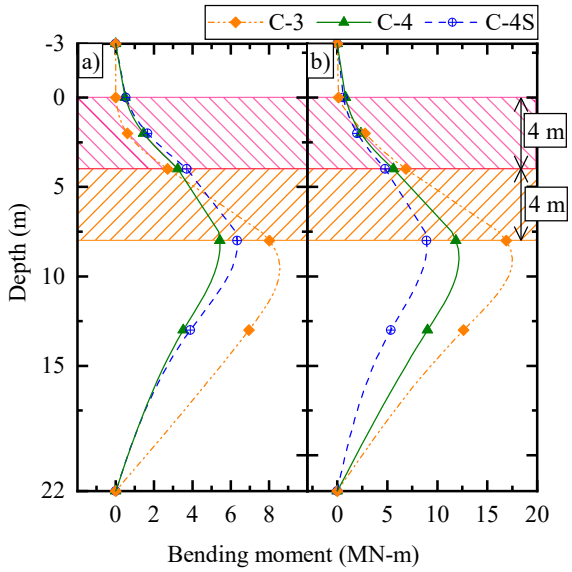

Fig. 21: Comparison of bending moment profiles of sheet pile in C-3, C-4, and C-4S while the sheet pile experiences maximum bending moment under; a) Tohoku Earthquake and b) sinusoidal waves.

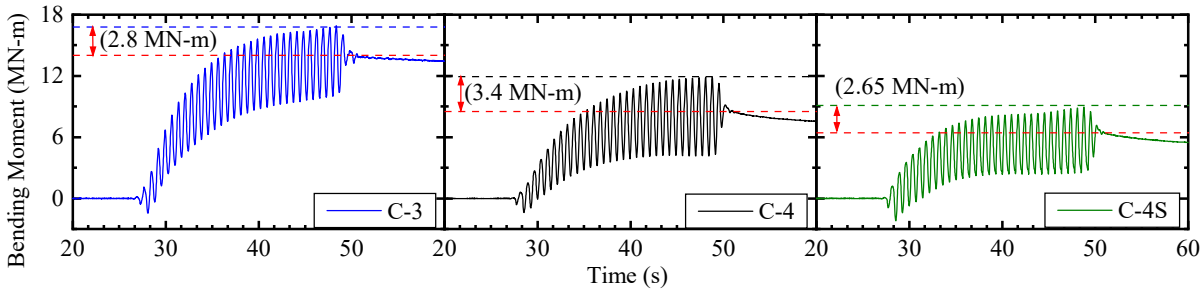

Fig. 22: Bending moment time history of the sheet pile where the sheet pile experiences maximum bending moment (SP-4) in C-3, C-4, and C-4S.

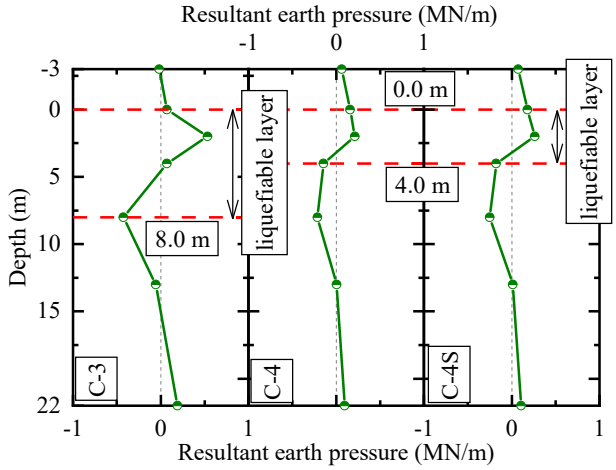

Fig. 23: Resultant earth pressure profiles in C-3, C-4 and C-4S when the sheet pile experiences maximum bending moment during Tohoku Earthquake.

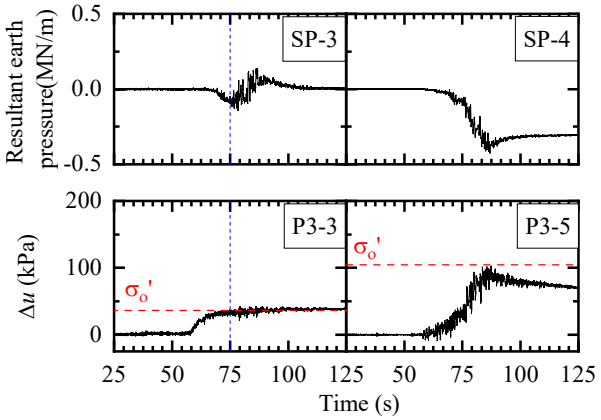

Fig. 24: Time histories of resultant earth pressure at SP-3 and SP-4 and the excess pore water pressure (Δu) inside the river channel for C-3.

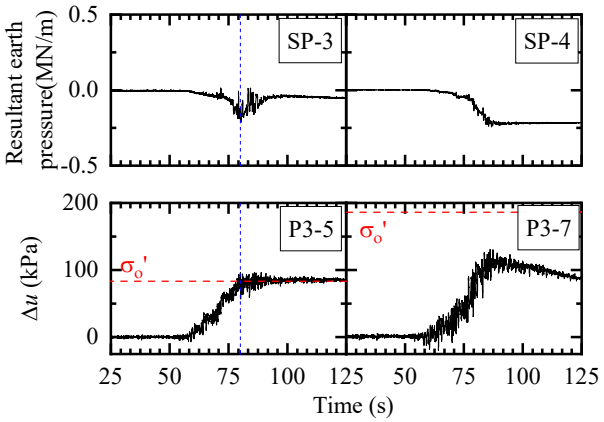

Fig. 25: Time histories of resultant earth pressure at SP-3 and SP-4 and the evolution of excess pore water pressure (Δu) inside the river channel for C-4.

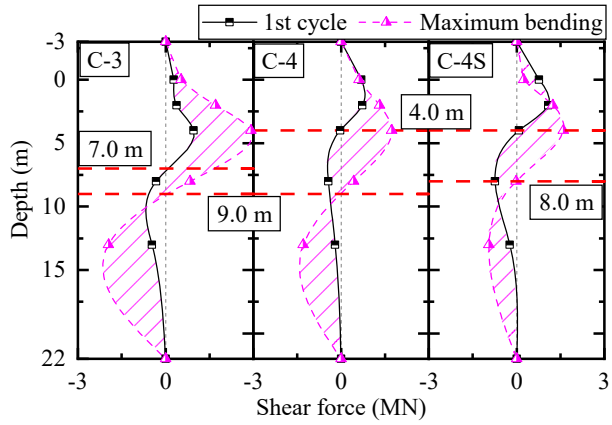

Fig. 26: Shear force distributions at the cyclic peaks of the 1st cycle and the maximum bending event during sinusoidal waves.